

**Supporting Information: Thermal conductance across phosphonic acid molecules and interfaces: ballistic versus diffusive vibrational transport in molecular monolayers**

John T. Gaskins,<sup>1</sup> Anuradha Bulusu,<sup>2</sup> Anthony J. Giordano,<sup>3</sup> John C. Duda,<sup>1,4</sup> Samuel Graham,<sup>2,\*</sup> Patrick E. Hopkins<sup>1,\*</sup>

1. Department of Mechanical and Aerospace Engineering, University of Virginia, Charlottesville, VA 22904, USA

2. Woodruff School of Mechanical Engineering, Georgia Institute of Technology, Atlanta, Georgia 30332, USA

3. School of Chemistry and Biochemistry, Georgia Institute of Technology, Atlanta, Georgia 30332, USA

4. Current Address: Seagate Technology, Bloomington, Minnesota 55435, USA

\* corresponding authors

phopkins@virginia.edu

sgraham@gatech.edu

## SUPPORTING INFORMATION

### *Metal/Phosphonic Acid/Sapphire Sample Characterization and Fabrication*

In order to address the orientation of the PA molecules on the sapphire surface, we examine studies on similar molecular structures. Gliboff *et al.*,<sup>1</sup> used near-edge X-ray absorption fine structure (NEXAFS) spectroscopy and density functional theory (DFT) based modeling to determine the orientation to the surface normal of aromatic and aliphatic phosphonic acids bound to indium tin oxide (ITO) substrates as a function of fluorination. The aromatic PA consisted of a phenyl phosphonic acid (PPA) with a fluorinated counterpart in F<sub>3</sub>PPA. Similarly, the aliphatic PA consisted of octyl phosphonic acid (OPA) with a fluorinated counterpart in F<sub>3</sub>OPA. In the case of OPA and F<sub>3</sub>OPA, they observed that the OPA molecule lies flatter than the F<sub>3</sub>OPA molecule ( $41 \pm 8^\circ$  for OPA vs.  $30 \pm 5^\circ$  for F<sub>3</sub>OPA) indicating a well-ordered system for the F<sub>3</sub>OPA. These values were similar to the values reported previously for alkanethiol and fluorinated alkanethiol SAMs on gold, despite the great difference in binding chemistry and surface mobility between thiols and phosphonic acids.<sup>2-3</sup> The authors attributed the more vertical orientation of the F<sub>3</sub>OPA molecule to an increase in the steric radius of the fluorinated chain as well as a decrease in the number of defects arising from the molecular orientation of the (CH<sub>3</sub>) methyl group (gauche defects). The authors theorized that since the fluorinated chains dominate the packing of the F<sub>3</sub>OPA molecule, similar vertical orientation can be expected for a fully fluorinated chain. Based on this argument, we expect to see similar vertical orientation of the F21PA molecule.

In contrast, in the case of the aromatic PAs, the non-fluorinated PPA showed a more vertical orientation of  $\sim 8^\circ$  ( $71 \pm 4^\circ$  for PPA) compared to  $63 \pm 4^\circ$  for the F<sub>3</sub>PPA. Through

density functional theory (DFT) based calculations, this difference was attributed primarily to the higher ratio of bidentate to tridentate bonding in the case of the F<sub>3</sub>PPA when compared to the PPA<sup>4</sup> with minimal van der Waals interaction between the fluorine atoms and the ITO surface. While similar experiments are outside the scope of this paper, following the same rationale, we expect similar tilt angles for the fluorinated, aromatic PFBPA molecules with 5 fluorine atoms.

Following the PA modification of the sapphire substrates, 90 nm thick films of various metals such as Al, Ni or Au were deposited on the substrates through electron beam evaporation using a Denton Explorer system. The deposition pressure was  $\sim 2 \times 10^{-6}$  Torr and the deposition rate was 1 Å/sec. In order to ensure that the metal deposition process did not cause any removal of PA molecules from the surface, a sapphire sample was modified with 3,3,4,4,5,5,6,6,7,7,8,8,8-tridecafluorooctyl phosphonic acid (FHOPA) containing 13 fluorine atoms using the spray coating technique described above. Five nanometers of Ni were deposited on the FHOPA modified sapphire substrate through electron-beam evaporation. Following Ni deposition, X-ray photoelectron spectroscopy (XPS) was used to determine the presence of F1s peak emitted by the fluorine atoms from the FHOPA molecule on sapphire underneath the ebeam deposited Ni layer. The choice of FHOPA molecule over PFBPA was due to the higher number of F atoms (13 F atoms) in the case of FHOPA that would allow for a higher intensity F1s signal beneath the 5 nm thick Ni film when compared to the PFBPA molecule (5 F atoms). Based on conventional ebeam studies, it is expected that a 5 nm thick Ni film would allow for a complete film coverage over the substrate while being thin enough for the ~9-10 nm

depth of penetration of the XPS at normal takeoff angles allowing us to study the interface of Ni/FHOPA/sapphire. XPS data was collected on a Kratos Axis Ultra Spectrometer with Al K- $\alpha$  X source (1486.69 eV). Each XPS spectra were obtained on a 110  $\mu\text{m}$  spot size at three different locations at normal takeoff angle.

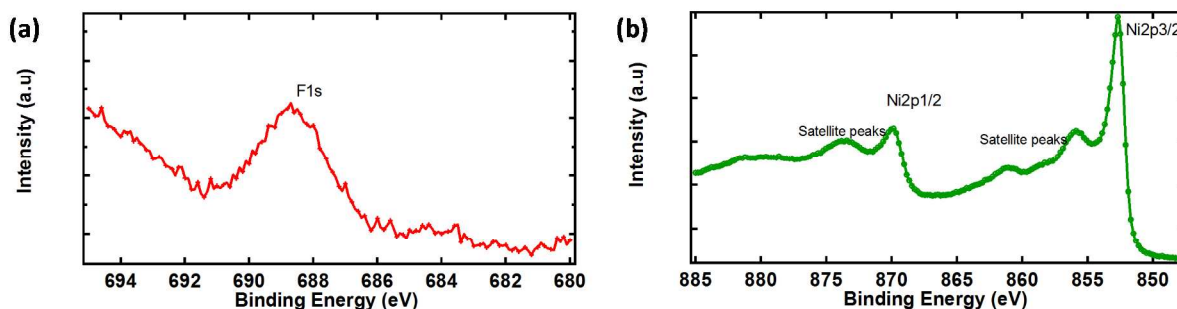


Figure S1. (a) F1s (a) and (b) Ni2p XPS peaks on  $\text{F}_{13}\text{OPA}$  modified sapphire substrates coated with 5 nm of Ni through ebeam deposition.

Figure S1a and S1b show the F1s and Ni2p XPS peaks respectively for  $\text{F}_{13}\text{OPA}$  modified sapphire substrates coated with 5 nm of Ni. It is evident from Figure S1a that there is a clear F1s peak underneath the 5 nm thick film validating that the phosphonic molecule is strongly bound to the sapphire substrate and was not removed during the metal deposition process.

**Synthesis of (3,3,4,4,5,5,6,6,7,7,8,8,9,9,10,10,11,11,12,12,12-Henicosafluorododecyl)phosphonic acid**

The (3,3,4,4,5,5,6,6,7,7,8,8,9,9,10,10,11,11,12,12,12-Henicosafluorododecyl)phosphonic acid (F21PA) molecule, shown in Fig. S2, was synthesized with the following procedure. In a 250 mL round bottom flask  $^1\text{H}$ ,  $^2\text{H}$ ,  $^2\text{H}$ -perfluoro-1-iodododecane (20.1 g, 29.8 mmol) was combined with triethyl phosphite (16 mL, 92.0 mmol) and the mixture was allowed to stir at 130 °C for 48 hours. Excess triethyl phosphite and other undesired side products were removed by heating at 85 °C under vacuum (approximately 0.1 Torr) overnight. A substantial amount of starting material sublimed, and was added back to the impure material. Triethyl phosphite was then added to the combination of unreacted starting material and impure product (45 mL, 258.6 mmol) and reacted at 135 °C for an additional 72 hours. Removal of excess triethyl phosphite under vacuum (80 °C, approximately 0.2 Torr) overnight afforded a brown, waxy solid. A portion of this solid was purified by silica gel column chromatography eluting with a mixture of 9:1 ethyl acetate:hexanes to afford diethyl (3,3,4,4,5,5,6,6,7,7,8,8,9,9,10,10,11,11,12,12,12-henicosafluorododecyl)phosphonate as a white solid (3.1 g, 15.2 %). The  $^1\text{H}$  NMR was consistent with that reported in the literature.<sup>5</sup>

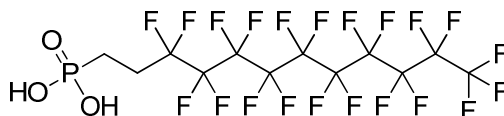


Figure S2. Molecular structure of F21PA

The phosphonate from the previous step was placed in a 250 mL round bottom flask (2.76 g, 4.0 mmol) and dissolved in anhydrous dichloromethane (approximately 25 mL). Bromotrimethylsilane (2.2 mL, 16.7 mmol) was added *via* syringe. The reaction vessel was sealed with a greased stopper and the mixture allowed to stir at room temperature

overnight. Volatiles were removed under reduced pressure and the resulting thick oil was dissolved in a 10:1 methanol:water solution, which was allowed to stir at room temperature for 6 hours. After removal of volatiles *in vacuo* a white solid was obtained which was recrystallized from methanol to obtain the title compound (1.4 g, 55.3 %).  $^1\text{H}$  NMR (399.96 MHz,  $\text{CD}_3\text{OD}$ )  $\delta$  2.43 (m, 2H), 1.94 (m, 2H).  $^{31}\text{P}$  NMR (161.91 MHz,  $\text{CD}_3\text{OD}$ )  $\delta$  26.51.  $^{19}\text{F}$  NMR (376.28 MHz,  $\text{CD}_3\text{OD}$ )  $\delta$  -80.47 (t,  $J = 7.5$  Hz, 2F), -114.50 (s, br, 3F), -120.80 (s, br, 10F), -121.80 (s, br, 2F), -122.57 (s, br, 2F), -125.37 (s, br, 2F). Elemental analysis calculated (found): C 22.95 (22.80), H 0.96 (0.89), F 63.52 (63.60). The  $^1\text{H}$  NMR was consistent with that reported in the literature.<sup>5</sup>

***Time domain thermoreflectance measurement sensitivities and uncertainty considerations***

In order to ensure sufficient sensitivity to the thermal boundary conductance between the metal and sapphire layers, we characterize how sensitive the ratio of the in-phase to out-of-phase components of the lock-in amplifier are to the thermophysical properties of various resistance in our sample, shown in Fig. S3. We calculate the sensitivity of our TDTR measurements to the thermal conductivity of the substrate, thermal conductivity of the transducer and thermal boundary conductance between these two layers using the procedure outlined previously<sup>7</sup>. Figures S23 and S3b show the sensitivity for nickel transducers with both low  $h_k$  ( $70 \text{ W m}^{-2} \text{ K}^{-1}$ ) and high  $h_k$  ( $200 \text{ W m}^{-2} \text{ K}^{-1}$ ), corresponding to sensitivity to F21PA at the interface and all other nickel coated samples, respectively.

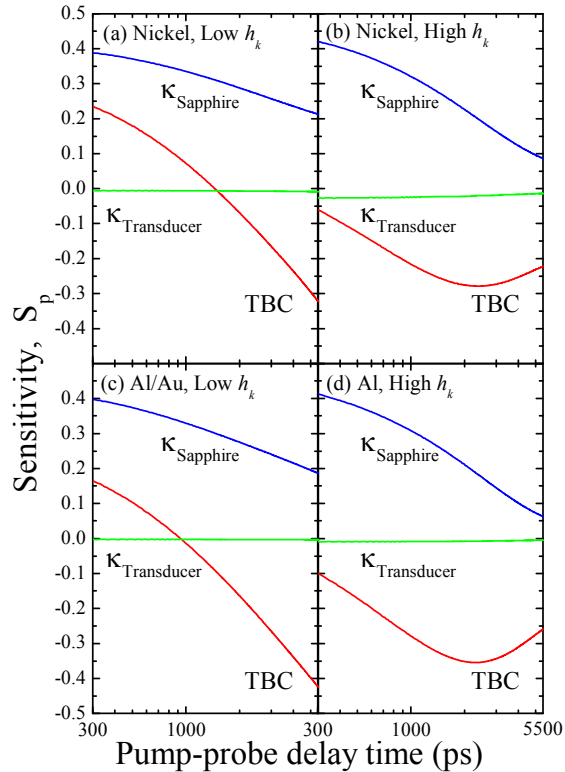


Figure S3. Sensitivity of relevant thermophysical parameters as a function of the pump-probe delay time used for our measurement. The four cases shown here characterize all combinations of metal transducer and  $h_k$  measured in this study. In the case of the gold transducer, the low case is the relevant sensitivity analysis for both measurements on gold transducers.

The sensitivity to all gold-coated samples and the aluminum sample with F21PA at the interface is shown in Fig. S3c, with a corresponding  $h_k$  of  $65 \text{ MW m}^{-2} \text{ K}^{-1}$ . The similarity in thermal properties between gold and aluminum allow us to make this generalization, while the differing heat capacity and thermal conductivity of nickel require its own sensitivity analysis. Figure S3d represents the sensitivity to measurements with no PA at the interface and all other PAs, exclusive of F21PA, with a  $h_k$  of  $160 \text{ MW m}^{-2} \text{ K}^{-1}$ . These sensitivity analyses show that we are sensitive to both the thermal conductivity of the sapphire substrate and the thermal boundary conductance across the metal/substrate

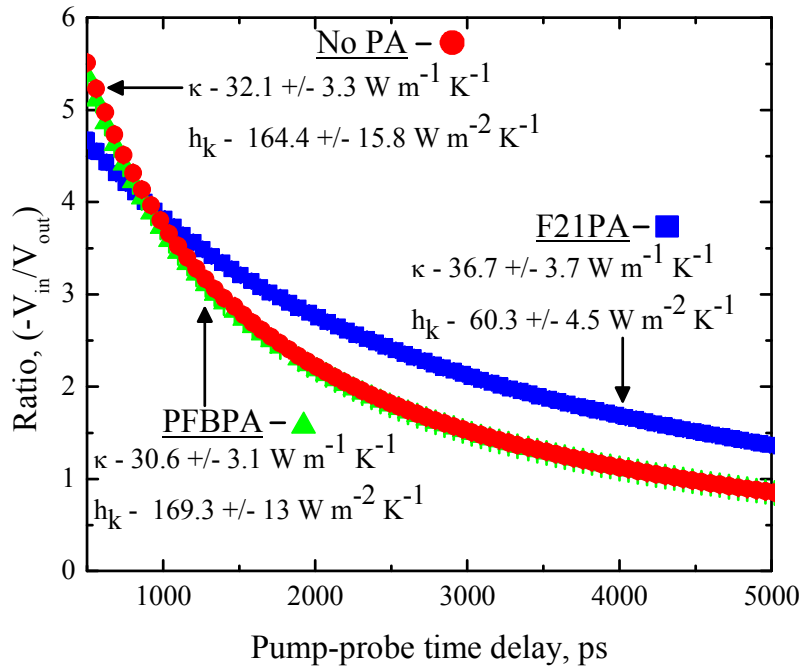


Figure S4. Averaged data from three exemplary tests each on Al/sapphire (circles), Al/PFBPA/sapphire (triangles) and Al/F21PA/sapphire (squares). The fit to the data and standard deviation from tests are smaller than the data points. Values from error are largely due to uncertainty in the thickness of the metal transducer and not from test to test repeatability.

boundary. This provides a secondary check as to the validity of our measurement, as we fit not only the thermal boundary conductance between the metal and sapphire, but also

the thermal conductivity of the sapphire substrate, which is commonly found to be between 30 and 40 W m<sup>-1</sup> K<sup>-1</sup> in literature.<sup>8</sup>

Figure S4 demonstrates the test-to-test repeatability of our measurements, displaying the average of three exemplary measurements taken on different locations of the sample. In each case presented in Fig. S4, Al/sapphire, Al/PFBPA/sapphire and Al/F21PA/sapphire, the standard deviation for the three tests is smaller than the data points graphed. The standard deviation from the mean in both the manuscript and the values in Fig. S4 is mostly due to uncertainty in the thickness of the metal transducer, taken as +/- 3nm for all computed data. There is a clear differentiation between the F21PA interface and both no PA and PFBPA at the interface, which extends to both the gold and nickel transducers (not shown). Additionally, Fig. S4 demonstrates the negligible relative change between the no PA samples and the PFBPA sample. It should be noted that the difference between the metal/sapphire control and non-F21PA PAs, seen in Fig. 4 in the main manuscript, may also be attributed to uncertainty in the transducer film thickness. The standard deviation in  $h_K$  for all metal/PA/sapphire measurements, excluding F21PA, falls within the standard deviation of the metal/sapphire control samples.

It is important to note that the changes in error for thermal boundary conductance values scale with the magnitude of the thermal boundary conductance. For instance, although the Al only error in Fig. 5 are significantly higher than the other values, the error for these samples relative to the magnitude of the reported conductance are very similar. Indeed, when we examine the error in thermal boundary conductance measurements of

these room temperature Al only data to those presented in Fig. 3, all of the reported error for samples with thermal boundary conductance of similar magnitude is comparable.

## References

1. Gliboff, M.; Li, H.; Knesting, K. M.; Giordano, A. J.; Nordlund, D.; Seidler, G. T.; Brédas, J.-L.; Marder, S. R.; Ginger, D. S., Competing Effects of Fluorination on the Orientation of Aromatic and Aliphatic Phosphonic Acid Monolayers on Indium Tin Oxide. *J. Phys. Chem. C* **2013**, *117*, 15139-15147.
2. Alloway, D. M.; Hofmann, M.; Smith, D. L.; Gruhn, N. E.; Graham, A. L.; Colorado, R.; Wysocki, V. H.; Lee, T. R.; Lee, P. A.; Armstrong, N. R., Interface Dipoles Arising from Self-Assembled Monolayers on Gold: Uv-Photoemission Studies of Alkanethiols and Partially Fluorinated Alkanethiols. *J. Phys. Chem. B* **2003**, *107*, 11690-11699.
3. Alves, C. A.; Porter, M. D., Atomic Force Microscopic Characterization of a Fluorinated Alkanethiolate Monolayer at Gold and Correlations to Electrochemical and Infrared Reflection Spectroscopic Structural Descriptions. *Langmuir* **1993**, *9*, 3507-3512.
4. Gliboff, M.; Sang, L.; Knesting, K. M.; Schalnat, M. C.; Mudalige, A.; Ratcliff, E. L.; Li, H.; Sigdel, A. K.; Giordano, A. J.; Berry, J. J., Orientation of Phenylphosphonic Acid Self-Assembled Monolayers on a Transparent Conductive Oxide: A Combined Nexafs, Pm-Irras, and Dft Study. *Langmuir* **2013**, *29*, 2166-2174.
5. Kraft, U.; Zschieschang, U.; Ante, F.; Kalblein, D.; Kamella, C.; Amsharov, K.; Jansen, M.; Kern, K.; Weber, E.; Klauk, H., Fluoroalkylphosphonic Acid Self-Assembled Monolayer Gate Dielectrics for Threshold-Voltage Control in Low-Voltage Organic Thin-Film Transistors. *J. Mater. Chem.* **2010**, *20*, 6416-6418.
6. Ghaemy, M.; Bazzar, M.; Berenjestanaki, F. R., Curing of Dgeba/Zno Nanocomposite with New Fluorinated Curing Agents Study of Kinetics, Water

Absorption, Thermal and Photophysical Properties. *High Perform. Polym.* **2012**, *24*, 632-645.

7. Costescu, R. M.; Wall, M. A.; Cahill, D. G., Thermal Conductance of Epitaxial Interfaces. *Phys. Rev. B* **2003**, *67*, 054302.

8. Auerkari, P., *Mechanical and Physical Properties of Engineering Alumina Ceramics*; Technical Research Centre of Finland Finland, 1996.